Discrete element modeling of the influence of void size and distribution on the mechanical behavior of rock

A.Fakhimi, Ph. D.
Department of Mineral Engineering, New Mexico Tech, Socorro, NM, USA
Department of Civil Engineering, Tarbiat Modares University, Tehran, Iran

E.A. Gharahbagh, Graduate Student
Department of Mineral Engineering, New Mexico Tech, Socorro, NM, USA

ABSTRACT: The effect of porosity on mechanical behavior of rock has been studied in the past using both experimental and numerical techniques. One important aspect of this study that has not received much attention is the role of void size and distribution on the mechanical behavior of rock. In this study, the CA2 computer program that is a hybrid discrete-finite element program for two-dimensional simulation of geomaterials is used. Numerical specimens with different macro-void sizes are loaded uniaxially. The Young's modulus, Poisson's ratio, uniaxial strength and crack initiation stress are studied. The numerical results are compared with the database of experimental tests on Plaster of Paris specimens containing Styrofoam spheres with different void sizes and porosities. It is shown that the macro void spatial distribution is partly responsible for the scatter of the experimental data. It is also shown that not-only the porosity but also the pore size can affect the deformability, crack initiation stress and rock strength.

1 INTRODUCTION

Different variables such as pore pressure, fissures, sample size, temperature and porosity can affect the mechanical behavior of rock. The presence of voids has a considerable effect on engineering properties of rock such as uniaxial compressive strength, Young's modulus and Poisson's ratio. Several experimental and numerical studies have been conducted to investigate the effect of porosity on mechanical behavior of rock. Al-Harthi et al. 1999 studied the effect of porosity on the properties such as uniaxial strength and longitudinal wave velocity of vesicular basalt in Saudi Arabia. Avar et al. 2003 explored the effect of macroporosity on tuff. Palchik (2006) examined the role of porosity on the elastic modulus, friction angle and cohesion of porous sandy shales. His studies showed that both friction angle and cohesion reduce as the porosity increases. Erfourth et al. 2006 investigated the effect of large voids on the Young's modulus of rock like material by using numerical and experimental approaches. In the numerical simulation, the continuum mechanics codes were used. The pores were simulated by removing the material from the numerical domain at random locations. Schopfer et al. 2009 studied the effect of porosity on the elasticity, strength, and friction angle of cohesive granular materials numerically. The PFC3D discrete element code was used in their investigation. They concluded that both Young's modulus and strength decrease by increasing the porosity while Poisson's ratio is almost independent from the porosity. Potyondy (2007) studied the effect of pore shape using a two-dimensional discrete element analysis. In his investigation, it was demonstrated that pores with edges have greater impact on the stiffness and strength of the simulated material compared to the situation that pores are circular in shape. This finding is consistent with the theoretical investigations (Jaeger et al. 2007).
The objective of this paper is to investigate the effect of macro void distribution on the uniaxial compressive strength, Young's modulus, and Poisson's ratio through numerical modeling. The

effect of macro pore size is studied as well. The numerical results are compared with some published experimental findings that were obtained by conducting tests on rock like material. Rock like material such as Plaster of Paris specimens containing spherical Styrofoam inclusions are of interest as natural rocks are usually dissimilar in structure and are harder to sample and test. Different studies have used plaster to represent rock (Hudyma et al. 2004, Stimpson 1970, and Lajtai and Lajtai, 1975).

2 NUMERICAL MODEL

Numerical modeling offers a convenient way for better understanding the relationships between index properties of rock. By using the numerical modeling, the role of individual parameters can be examined while keeping all other parameters constant. This opportunity is rarely possible with rock specimens and laboratory measurements.

In this study, the CA2 computer program (Fakhimi, 1998) which is a hybrid discrete-finite element program for two-dimensional simulation of geomaterials is used. The rock is modeled as a bonded particle system. The rock grains are assumed as circular cylinders that interact through normal and shear springs. The cylinders are bonded to each other at the contact points in order to withstand deviatoric stresses. Each numerical sample of this study is 4 × 8 cm in dimension. To obtain numerical samples with different porosity, two different sets of cylinders are generated. The first set, macro void cylinders, is made of cylinders that represent the macro pore spaces. The second set of cylinders, grain cylinders, is to model the rock grains. The grain cylinders are generated by assuming a uniform random distribution for their radii (with a range of 0.4 to 0.6 mm) while the macro void cylinders are assumed to have a constant radius. Two different scenarios are considered in order to study the effect of macro pore size on the rock strength. In the first scenario, the macro void cylinders have a radius equal to the average grain radius (0.5 mm). In the second situation, the radius of macro void cylinders is assumed to be equal to five times the average grain radius (2.5 mm). To prepare a numerical specimen, the surrounding finite element domain is generated initially. The finite element grid acts as a mold for holding the discrete particles. The macro void cylinders are then generated. The location of each macro void cylinder is randomly selected using a uniform random number generator. Lastly, the grain cylinders are generated. The cylinders are smaller in size initially to be able to accommodate them in the domain of analysis. After the generation of cylinders, they are inflated to their final radii and the equations of motion together with linear contact laws are solved to adjust the location of grain cylinders and to distribute the micro void spaces more uniformly. At this stage, the cylinders are not bonded at the contact points and are friction free but the macro void cylinders are held fix in their position to control the macro void positions and distribution within the numerical sample. This sample preparation procedure provides a genesis pressure (σ_0) that is the required surrounding pressure by the frictionless walls to hold the required dimension of the numerical specimen (4 × 8 cm). After sample preparation, the initial stresses, contact forces, and velocity vectors are initialized to zero, normal and shear bonds and friction are introduced at the contact points, and the macro-void cylinders are deleted from the numerical sample. Through this approach, with a relatively small effort, samples with different macro-void distribution and size are generated.

The micro-mechanical constants adopted for the numerical model are shown in Table 1. Figure 1a shows the sample size and the macro void cylinders. In Figure 1b, the final numerical specimen after removal of the macro void cylinders is shown. Figure 2 shows a numerical specimen under uniaxial loading. The upper and lower loading platens are modeled using finite elements. The top of upper platen is fixed in vertical direction while the lower platen moves with a constant quasi-static velocity of 0.2×10^{-8} m/cycle. The walls or interfaces between the platens and the grain cylinders are assumed to be frictionless. The axial deformation and stress in the numerical specimen together with the porosity and number of micro-cracks are recorded during the specimen loading for further analysis. Lateral deformations at the mid height of the specimen at both sides are measured using two finite element domains that are glued to the discrete cylinders at the contact points (Figure 2). A small elastic modulus is introduced for these two

Table 1. Micro mechanical properties for interaction of cylinders at the contact points.

Micro mechanical property	Value
Normal spring stiffness (k_n)	84.8 MPa
Shear spring stiffness (k_s)	35.6 MPa
Normal bond (n_b)	38.1 kN/m
Shear bond (s_b)	189.9 kN/m
Coulomb friction coefficient (μ)	0.5
Average of normalized genesis pressures (σ_0/k_n)	0.02

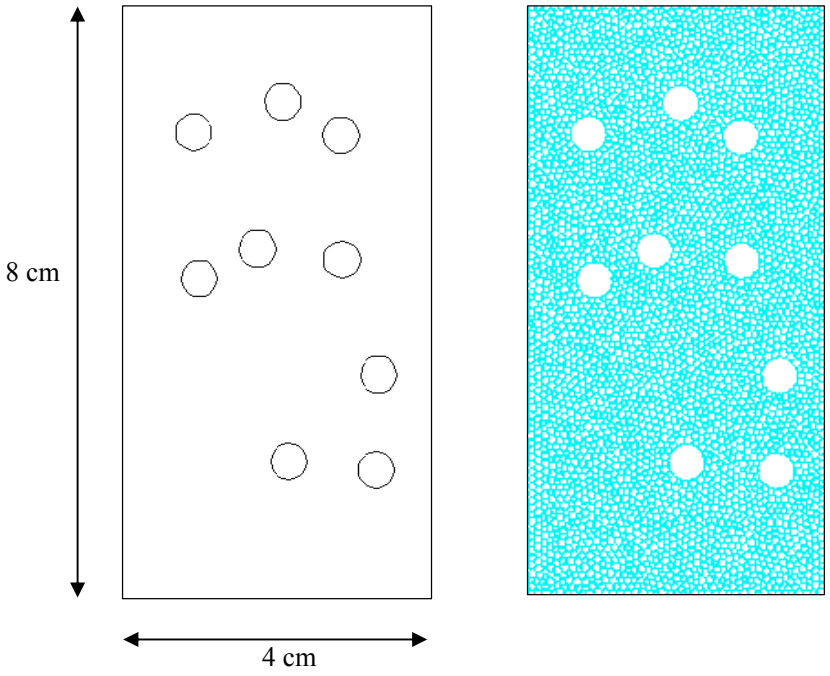

Figure 1. (a) Macro void cylinders; (b) final numerical specimen after removal of the macro void cylinders.

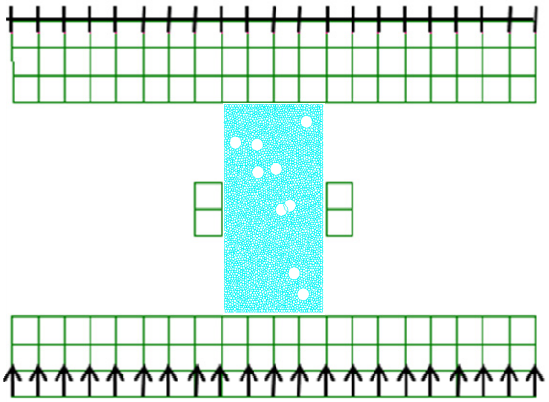

Figure 2. Numerical specimen under uniaxial loading.

finite element domains to prevent any artificial resistance of the material. The x-displacement component of the grid points in contact with the cylinders, at both left and right sides of the specimen, is used as a measure of lateral deformation of the specimen. The lateral deformation is used to calculate the Poisson's ratio of the numerical specimen.

Numerical uniaxial tests were conducted to investigate:

- The effect of macro-pore distribution on the mechanical behavior of the specimens
- The role of porosity change on the elastic properties and uniaxial strength of the specimens
- The effect of macro pore size on the specimens behavior
- The porosity change during the sample loading, crack initiation stress, and the number and location of developed cracks

3 NUMERICAL TESTS RESULTS

Numerical samples with two different macro-void sizes of R_{void} (void radius) equal to five times the average grain radius and equal to average grain radius were generated, i.e. R_{void} = 2.5 and 0.5 mm were adopted. Figure 3 shows the distribution of the macro-voids in a sample with an overall porosity of 16% and macro-voids of 2.5 mm in radius. Figure 3a, corresponding to the uniaxial stress of 46.2 MPa (68% of peak stress) indicates that as expected the micro-cracks were initiated in the vicinity of the macro-voids. By increasing the applied axial load, further micro-cracks developed in the specimen. Figures 3b and 3c show the micro-cracks at axial stresses of 64.5 MPa (95.3% of peak stress) and 67.7 MPa (peak stress), respectively. Similar micro-crack patterns in a specimen with a porosity of 16.8% and with the macro-voids radius of 0.5 mm are shown in Figure 4. The stress-strain curves for these two numerical specimens are shown in Fig. 5. Note that both specimens have relatively similar porosities, but the macro-pore sizes are different. Figure 5 suggests that both the Young's modulus and uniaxial compressive strength for the specimen with larger macro voids are greater than those of the other specimen. The crack initiation stresses for both specimens are shown with circular symbols on the stress-strain curves. It appears that the initial micro-cracks start at earlier stages, with respect to the uniaxial strength values, for the specimen with larger pores. This can be due to the greater deformation concentration around the larger pores as the existence of more grains around a single macro-void provides a greater number of degrees of freedom for the rigid grains.

In Figure 6, the number of induced micro-cracks is shown. The two circular symbols correspond to the points that crack generation rate increases suddenly and to the peak stress for each specimen. Note that Figures 3b and 4b are showing the induced cracks at axial stresses corresponding to the points of high crack generation rate. These figures suggest that majority of micro-cracks are developed at compressive stresses that are very close to the peak stresses. In Figure 7, the lateral displacements for the left and right mid-height points of the specimens are shown. Notice the initial linear lateral deformation with axial displacement up to the crack initiation points (the leftmost circular symbols). By further deformation of the specimens, the lateral deformation starts to deviate from a linear behavior. This rate is the greatest when the micro-crack generation rate increases toward the peak stress. Notice that the lateral deformation of the specimen with the larger macro pore size is greater than that of the other specimen. This is consistent with the greater micro-crack generation in this specimen (Fig. 6).

In Figure 8, the porosity change versus the axial strain is shown. As expected, up to the crack initiation points, the porosity reduces due to the compressive stresses and the elastic behavior of the specimens. After the crack initiation points, a competition starts between the elastic compression of the pores and the dilatational deformations due to crack propagation. This causes a reduction in the rate of porosity change after the crack initiation stresses which are followed by an increase in porosity after the points of high rate of micro-crack generation and subsequently peak stresses are approached. It is interesting to note that the porosity change in the specimen with larger macro voids is greater than that for the specimen with smaller macro pore size.

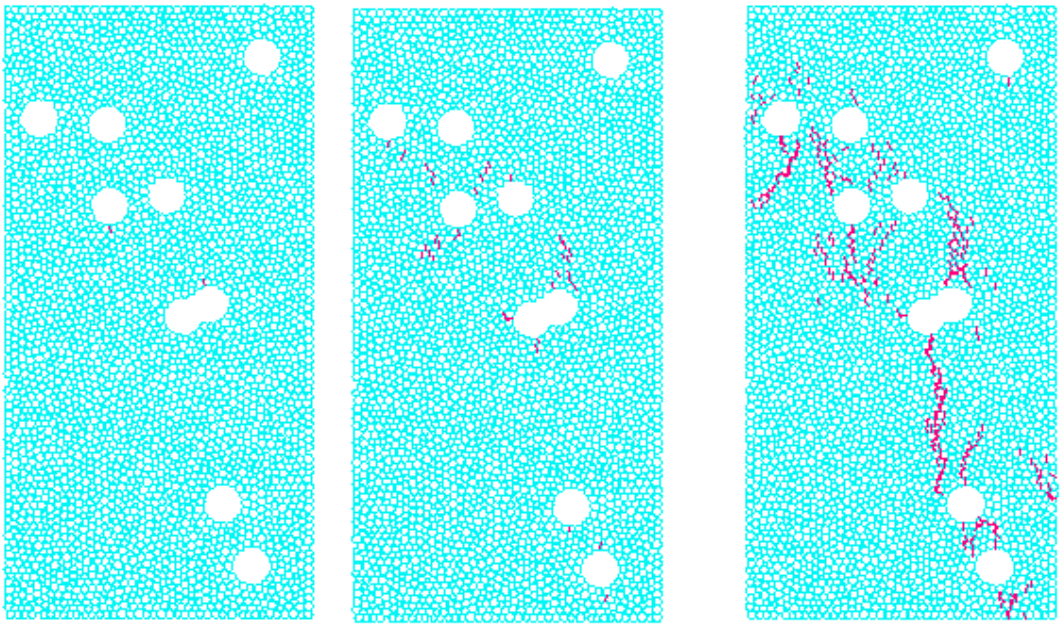

(a) (b) (c)

Figure 3. Micro-cracks in a numerical specimen with an initial porosity of 16% and a macro-pore radius of 2.5 mm at an axial stress of (a) 68% of peak stress, (b) 95.3% of peak stress, and (c) 100% of peak stress (67.7 MPa).

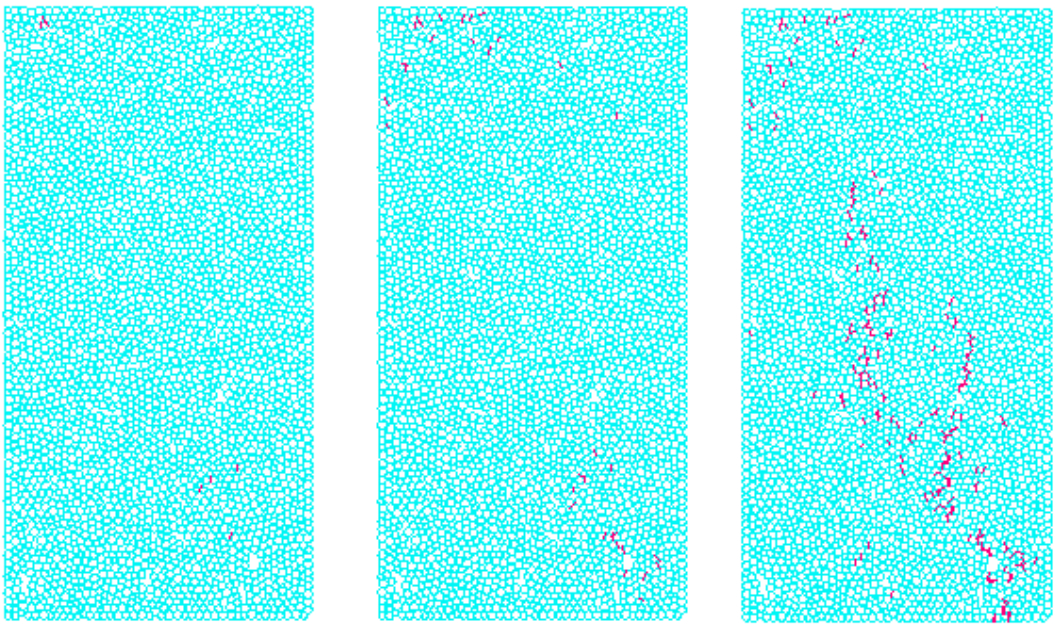

(a) (b) (c)

Figure 4. Micro-cracks in a numerical specimen with an initial porosity of 16.8% and a macro-pore radius of 0.5 mm at an axial stress of (a) 86% of peak stress, (b) 99.8% of peak stress, and (c) 100% of peak stress (44.1MPa).

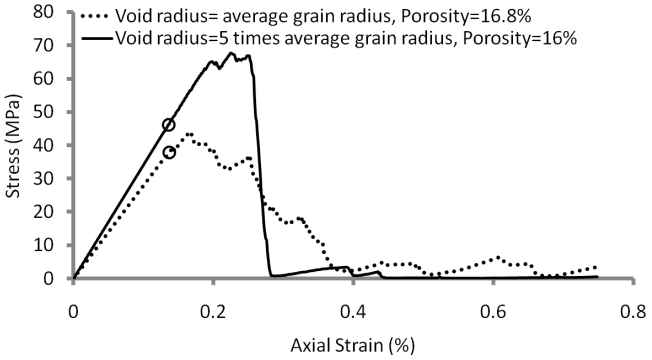

Figure 5. Stress-strain curves for numerical specimens with different macro-void sizes.

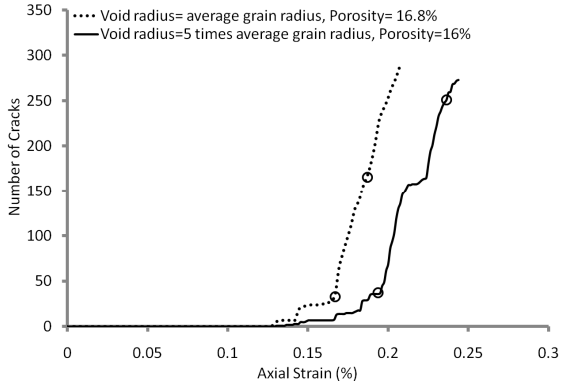

Figure 6. Number of micro-cracks versus axial strain for numerical specimens with different macro-void sizes.

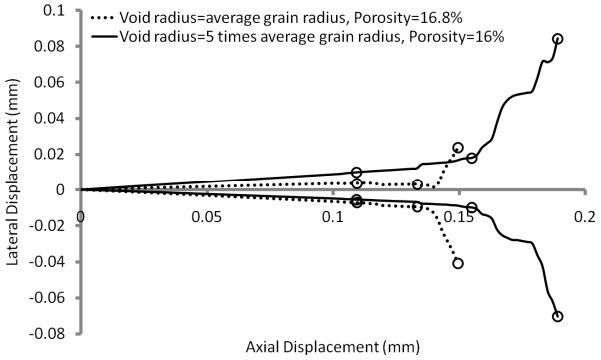

Figure 7. Lateral displacement versus axial displacement for numerical specimens with different macro-void sizes.

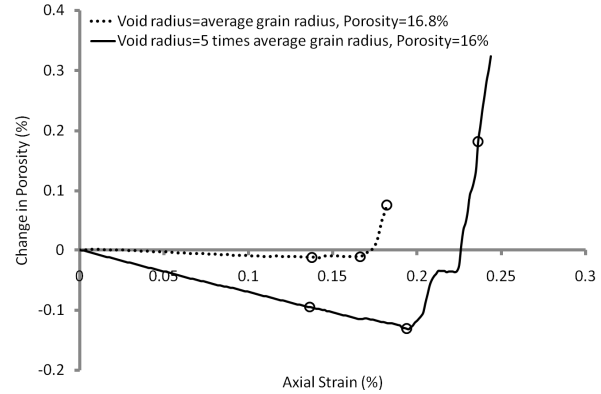

Figure 8. Porosity change versus axial strain for numerical specimens with different macro-void sizes.

To investigate the effect of macro void distribution on the elastic modulus and uniaxial strength, fifty numerical specimens with the porosity of 16% and macro void radius of 2.5 mm and fifty specimens with the porosity of 16.8% and macro void radius of 0.5 mm were generated. For each numerical specimen, a uniform random number generator was used to find the x and y coordinates of the center of each macro void cylinder. Macro voids were prevented to have overlaps even though in some samples small overlaps were unavoidable after inflation of the cylinders to their final size. Figures 9 and 10 show the histograms for the Young's modulus and uniaxial strength of specimens with large and small macro pore sizes, respectively. The mean and coefficient of variation values for the Young's modulus and uniaxial strength of specimens with large and small macro void sizes are (32.5 GPa, 11%; 73.1 MPa, 17.5%) and (25.5 GPa, 4.2%; 43.0 MPa, 13.1%), respectively. Note that specimens with larger macro void size are both stiffer and stronger but they show greater variation around mean values of Young's modulus and uniaxial strength. This is consistent with the fact that for the same porosity value but larger macro pore sizes, the sample has a greater chance of being non-homogeneous in the distribution of the macro pore locations. This finding suggests that samples with larger pore size must be greater in dimension if a Representative Volume Element (RVE) is to be obtained.

In Figure 11, the histograms of crack initiation stress for samples with large and small macro pore sizes are shown. The crack initiation stress for samples with larger macro pore size shows greater scatter with a range of 15% to 71% of uniaxial strength. The crack initiation stress for specimens with smaller macro pore size is within 40% to 78% of uniaxial strength. These ranges can be compared with the crack initiation stress of Lac du Bonnet granite with reported values within 20% to 40% of uniaxial compressive strength (Martin, 1993).

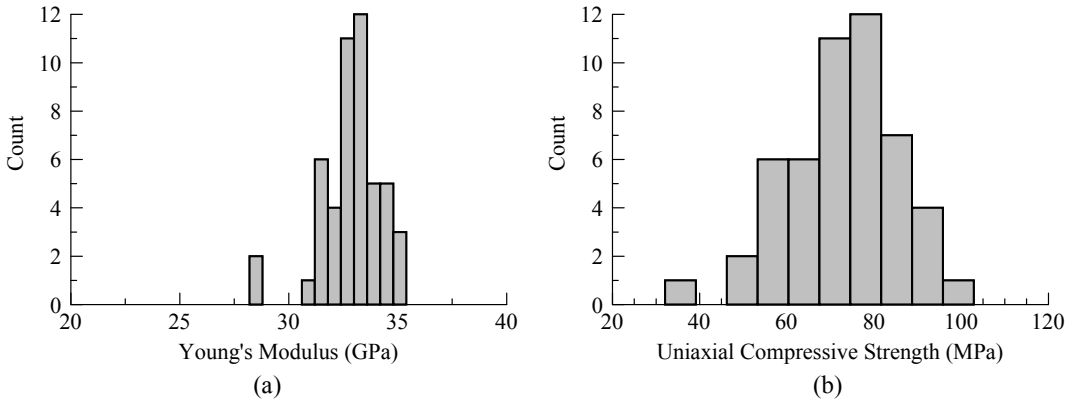

Figure 9. Histograms of: (a) Young's modulus, (b) uniaxial strength of specimens with a porosity of %16 and a macro void radius of 2.5 mm.

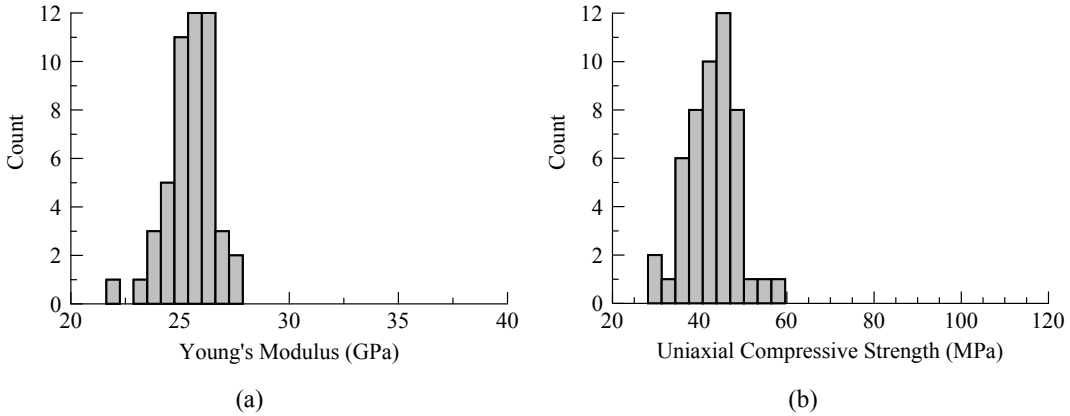

Figure 10. Histograms of: (a) Young's modulus, (b) uniaxial strength of specimens with a porosity of %16.8 and a macro void radius of 0.5 mm.